Physics – Uspekhi **52** (11) 1127 – 1137 (2009)

P N LEBEDEV PHYSICAL INSTITUTE — 75 YEARS

PACS numbers: 01.30.Bb, 95.55.Jz, 95.85.Bh, 95.85.Fm, 97.60.Gb

Radioastron: a radio telescope many times the size of Earth. Research program

N S Kardashev

DOI: 10.3367/UFNe.0179.200911e.1191

Abstract. A number of ground-based radio telescopes and one in a terrestrial orbit with the apogee at about the Earth–Moon distance have been combined to make an interferometer that provides the angular resolution up to a few microarcseconds for exploring astronomical objects such as pulsars, star formation regions, and black holes. Black hole horizon physics, cosmic ray acceleration regions, and the hypothetical wormhole entrances are becoming accessible to study for the first time.

Radio astronomy at LPI started with two permanently working expeditions in the Crimea. Several stations were organized to carry out radio astronomical observations: the main and biggest one was located near Simeiz (on Koshka Mountain near the village of Katsiveli), where the largest radio telescopes at that time were mounted.

Figure 1 presents photos of the founders of radio astronomy at LPI [1–4]. N G Basov and A M Prokhorov visited the Crimean expedition each summer and helped in organizing all work. In Moscow and in the Crimea, I S Shklovsky regularly discussed the most interesting research programs of radio astronomical observations with his LPI colleagues. However, the first scientific results were obtained in an expedition not on the ground but on board a ship. The program was headed by S E Khaikin, with the participation of V L Ginzburg and I S Shklovsky. The expedition on board the ship *Griboedov* journeyed to Brazil (the Bahia Bay) to observe the solar eclipse. Before that, Ginzburg made estimations showing that thermal radio emission from the Sun is generated in the solar corona, which was confirmed by observations with the radio telescope on board *Griboedov*. P D Kalachev was the principal designer of the largest radio telescopes that where constructed by the Crimean expedition and later at the Pushchino Radio Astronomical Observatory. After Khaikin, V V Vitkevich headed the radio astronomy department that handled the new radio telescopes and radio interferometers of LPI. In Pushchino, A E Salomonovich, together with Kalachev, constructed the world's largest reflector radio telescope with the diameter 22 meters operating at the mm and cm wavelengths.

N S Kardashev Astro Space Center, P N Lebedev Physical Institute, Russian Academy of Sciences,
ul. Profsoyuznaya 84/32, 117997 Moscow, Russian Federation
Tel. (7-495) 333 21 89, (7-495) 334 85 06. Fax (7-495) 333 23 78
E-mail: nkardash@asc.rssi.ru

Received 15 June 2009
Uspekhi Fizicheskikh Nauk **179** (11) 1191 – 1202 (2009)
DOI: 10.3367/UFNr.0179.200911e.1191
Translated by K A Postnov; edited by A M Semikhatov

Figure 1. Founders of radio astronomy at LPI.

Table 1. Main parameters of the Radioastron mission.

Band (λ, cm)	92	18	6.2	1.2 – 1.7
Bandwidth	4	32	32	32
Interferometer beam width (mas) for 350,000 km baseline	540	106	37	7.1 – 10
Flux sensitivity (σ, mJy) in units of ground-based GBT * antenna for 300 s integration time	10	1.3	2	5
* GBT, Green Bank Telescope.				

At present, the main projects of LPI include two ground-based radio telescopes: the multi-beam antenna array at meter wavelengths, which will be capable of a continuous simultaneous monitoring of the entire sky, and the full-revolving mm–cm radio telescope RT-70 on the Suffa plain in Uzbekistan. LPI and Roskosmos, in cooperation with other institutes, are currently developing two space radio telescopes, Radioastron and Millimetron, which are included as principal projects in the Federal Space Program.

The launch of the Radioastron space mission is planned in the next year [5]. In combination with ground-based radio telescopes, it will form the Earth–space radio interferometer. Its main characteristics are listed in Table 1. The objects to be studied by the Radioastron mission (Spektr-R) include:

- the nuclei of galaxies (synchrotron radiation, cosmic rays, megamasers, new physics);
- cosmology, dark matter, dark energy, space–time;
- star formation and planetary formation regions (masers);

Figure 2. (a) Testing the space radio telescope at Pushchino. (b) Participants of the International Radioastron mission conference near the flight model of the SRT at Lavochkin RPC (autumn 2008).

• stellar-mass black holes and neutron stars;
• the interstellar and interplanetary medium;
• the ultrahigh-precision space reference frame and fundamental astrometry;
• ultrahigh-precision ballistics and the gravitational field of Earth.

Figure 2 shows the space radio telescope (SRT) during testing at Pushchino and the Lavochkin Research and Production Corporation (RPC) and a picture of participants of the Radioastron international workshop in 2008.

The method of radio interferometry with arbitrarily large bases (including space interferometers) was suggested and actively developed at LPI [6]. From the very beginning of space research, the first interferometers were mounted in the Crimea. These interferometers were connected by cables and had an angular resolution many times that of an individual antenna. Interferometers ensured the high-precision landing of the first spacecraft on the surface of the Moon. Immediately after the first experience of measuring the precise coordinates of spacecraft, the idea emerged that it is possible to construct an interferometer without cables and to register the signal from a source at different points in space by using highly stable synchronizing generators and processing the recorded signal by remote computers independently of the time of observation.

Figure 3 shows the assumed orbit of the Radioastron space interferometer [7] that is evolving in a certain way due to the influence of the Moon. The mean orbital period is 9.5 days (the period varies from 7 to 10 days), the large semimajor axis is about 189,000 km, and the orbital inclination is 51°. The perigee distance varies from 10 to 70 thousand km, the apogee radius changes from 310 to 390 thousand km. Over three years, the normal to the orbital plane describes an oval in the sky with major and minor semiaxes 150° and 40°. Due to the evolution of the orbit, about 80% of the sources are found close to the orbital plane at some time, and it is therefore possible to obtain images of such sources with both high and moderate angular resolution.

It is assumed that in the shortest wavelength band of the Radioastron project (band K), the image multifrequency synthesis method (IMS) will be realized [8]. One channel with circular polarization will be operating at the frequency 22.232 GHz; another channel with the opposite circular

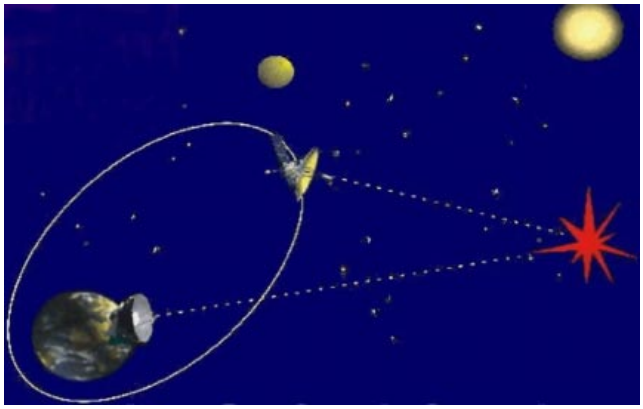

Figure 3. The orbit of the Radioastron space mission [7]. The mean orbital period is 9.5 days (the period changes from 7 to 10 days) , the major semiaxis is 189,000 km, the orbital inclination is 51.6°. The perigee and apogee distances vary from 10 to 70 and from 310 to 390 thousand km, respectively. The normal to the orbital plane describes an oval in the sky with major and minor axes 150° and 40°.

polarization can simultaneously switch in the frequency range 18.392–25.112 GHz, i.e., $f_{\max}/f_{\min} = 1.37$. This will enable simultaneously receiving images over the time interval determined by the integration time in each channel. Two-dimensional images can be obtained twice per orbital revolution with the maximum angular resolution and a 46% filling $[1 - (f_{\min}/f_{\max})^2 = 0.46]$ of the elliptical region on the UV-plane of space frequencies. It is important to note that these values are independent of the size or other parameters of the orbit. Generally, the fixed-frequency channel is fully consistent with that of ground-based radio telescopes. The switching frequency channel will also be consistent with the same band of the K-range of specially tuned ground-based radio telescopes.

Some advantages of the IMS method are as follows:

• one-dimensional source imaging with an extremely high angular resolution over less than one hour at any part of the orbit;
• two-dimensional imaging over 3–5 days at any part of the orbit or over 0.5–1 day close to the perigee;
• the possibility of obtaining a spectrum in the K-band for different details of the image;

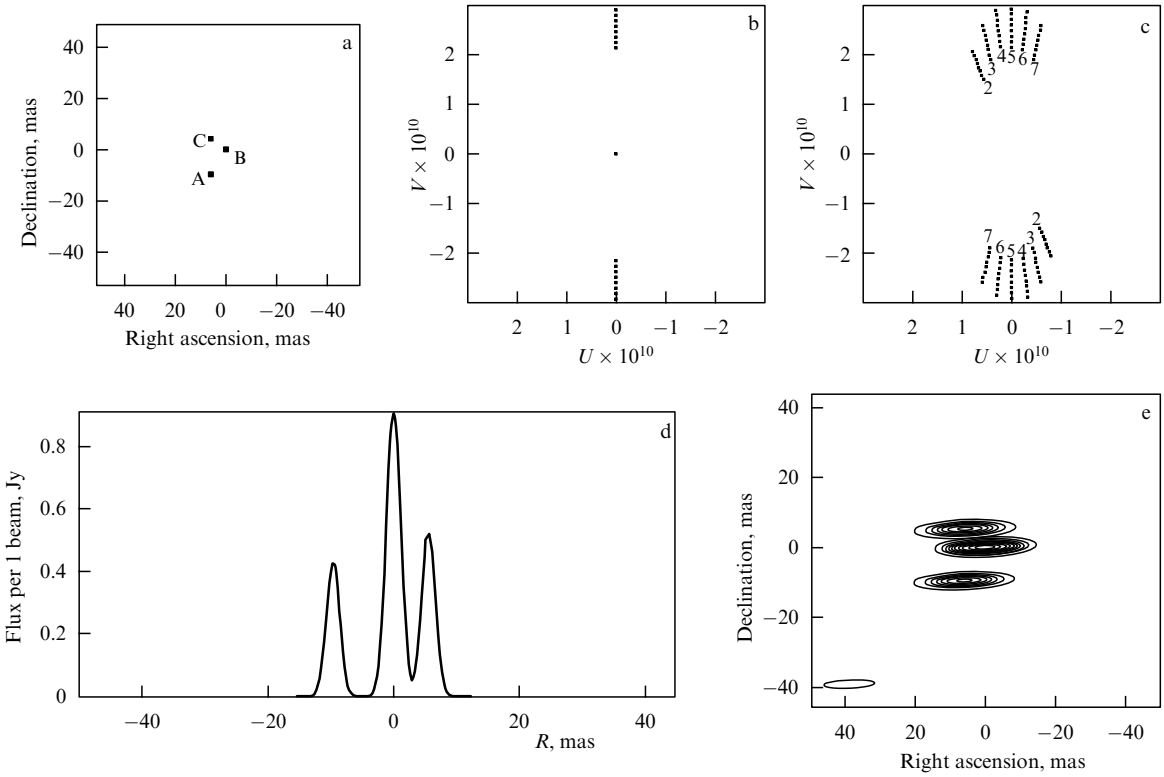

Figure 4. The IFS modeling method in the Radioastron mission [8]. (a) The true image consists of three point-like sources with fluxes $F_A = 0.5$, $F_B = 1.0$, and $F_C = 0.5$ in arbitrary units, AB = 12 μs, AC = 15 μs, and BC = 9 μs. (b) Filling of the UV-plane by switching eight frequencies in the K-channel, which results in a one-dimensional image (d). (c) Filling of the UV-plane by five switchings over five days, which yields a two-dimensional image (e).

• the determination of the angular diameter dependence on frequency due to scattering, absorption, or other physical processes;

• mapping of the linear polarization and Faraday rotation measures or circular polarization mapping, as well as the determination of the dependence of the polarization degree on frequency;

• the highly accurate determination of the differential coordinates and proper motion of the source;

• the possibility of studying the physical variability of the source structure and/or variability due to interstellar or near-source plasma as a function of frequency.

To address these goals, the corresponding mode of observations can be chosen at the channel central frequencies 18.392, 19.352, 20.312, 21.272, 22.232, 23.192, 24.152, and 25.112 GHz. The channel bandwidth at each frequency is 32 MHz.

Figure 4 shows the results of numerical simulation of one- and two-dimensional maps of a source consisting of three point-like components [8].

One of the principal research goals of the Radioastron space interferometer is to study the structure and dynamics of the central parts of extragalactic synchrotron radio sources, which could provide information from regions near the event horizon of supermassive black holes. Figure 5 shows a sky map with sources to be studied by the space radio interferometer. A large catalogue of sources has been prepared from observations at the Crimean and North-Caucasus observatories [9, 10]. Sources with different spectra are shown in different colors in Fig. 5. The most compact are the sources with inverted (i.e., increasing toward the high frequency) spectra (shown in green). Shown in red are less compact synchrotron sources with fluxes decreasing with frequency, or thermal sources with flat spectra (hot plasma clouds). An extended study of the structure of extragalactic sources and the determination of their components unresolved from the ground was carried out by the global VLBA (very long baseline array) interferometer at the frequency 15 GHz [11, 12]. Some of the strongest and most interesting compact sources are listed in Table 2.

Figure 6 shows the expected sizes of objects and the magnetic field structure in the nucleus of the radio galaxy Virgo A (M87). One of the biggest known supermassive black holes is thought to reside in the center of M87. The Radioastron mission will for the first time allow studying the structure of the innermost parts of this object, or even looking inside it (if it is not a black hole but, for example, the entrance to a wormhole). In Fig. 7, the characteristic sizes of the black hole model in M87 are shown. The minimum width of the interferometer beam is 7 mas, and depending on the signal-to-noise ratio, it will enable measuring the source size with an accuracy of a fraction of the beamwidth (for example, one decimal), i.e., it is expected to achieve an angular resolution better than one micro arcsecond. The expected size of the silhouette, i.e., the diameter of a circular orbit around a nonrotating black hole, is about 22 mas, which is three times as large as the beam size. If the black hole is rotating at the maximum, the silhouette diameter should be 19 mas, the right and left edges of the image must be respectively darker and brighter, and the brightness center must be shifted [13].

Figure 7 also shows 2 cm images [11, 12] and radio polarization data for quasar 3C 273 [14]. This object is one of the strongest radio sources. It is especially interesting for its

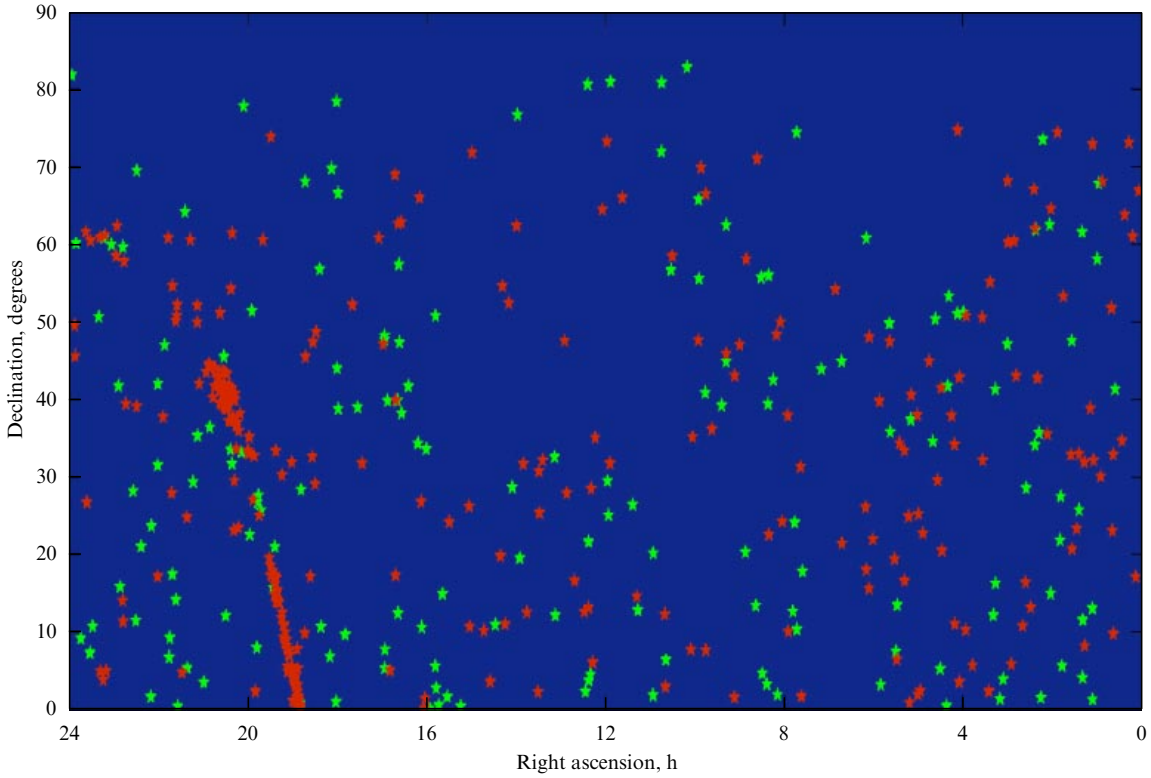

Figure 5. Radio sources in the northern hemisphere to be observed by the Radioastron telescope. Shown in red are sources with normal spectra, in green those with inverted spectra, probably the most compact [9]. (Color version online at http://www.ufn.ru.)

Table 2. The strongest and most compact extragalactic sources.*

IAU designation	Other names	z	S, Jy	$\Theta_{\max}$, mas	$\Theta_{\min}$, mas	T_b, 10^{13} K	N_0	N
0420-014		0.915	7.62	0.09	< 0.02	> 5.18	6	4
0528+134		2.07	4.21	0.22	< 0.03	> 2.06	6	3
0716+714		(0.3)	2.51	0.08	< 0.01	> 1.85	6	5
1055+018	4C+01.28	0.888	4.28	0.23	< 0.02	> 1.36	8	5
1334-127		0.539	7.17	0.16	< 0.01	> 3.19	6	4
1730-130	NRAO530	0.902	7.49	0.23	< 0.03	> 1.50	7	5
1741-038	OT-068	1.057	4.55	0.16	< 0.02	> 2.03	3	1
1749+096	4C+09.57	0.320	5.13	0.16	< 0.02	> 1.34	6	4
2230+114	CTA 102	1.037	3.11	0.12	< 0.03	> 1.27	9	5
2255-282		0.927	5.50	0.13	< 0.02	> 2.24	2	1
0642+449	OH471	3.408	1.67	0.21	0.08	0.43	6	4
0851+202	OJ 287	0.306	3.32	0.12	< 0.05	> 0.39	10	7
1226+023	3C273	0.158	7.36	0.13	< 0.06	> 0.17	15	11
1228+126	M87	0.004	0.73	0.41	< 0.27	> 0.007	13	5
1253-055	3C279	0.538	11.21	0.30	< 0.05	> 0.88	14	8
1508+572	VSOP	4.309	(0.1)					
1937-101		3.787	0.16	0.30	0,12	0,015	2	0
2200+420	BL Lac	0.069	2.78	0.37	< 0.03	> 0.15	14	10
2251+158	3C454.3	0.859	3.77	0.26	0.11	0.105	11	4

* IAU — International Astronomical Union, z — redshift, S — flux form unresolved source detail, $\Theta_{\max}$ and $\Theta_{\min}$ — maximum and minimum sizes, T_b — brightness temperature of a detail unresolved at the frequency 15 GHz, N_0 — the number of observational runs, N — the number of observational runs in which an unresolved detail was observed [11, 12].

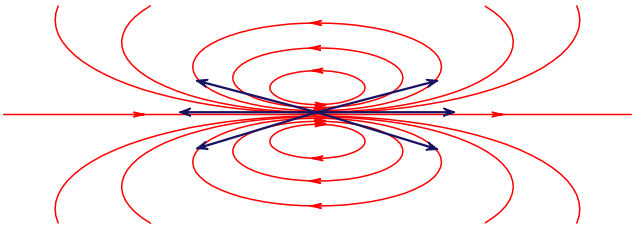

Figure 6. Magnetic field in the central regions of the radio galaxy M87: the dipole field of the accretion disk and the monopole field of the wormhole. The possible structure of M87 [13]. The distance is 16 Mpc, the black hole mass is $3.4 \times 10^9 M_\odot$. The Schwarcschild diameter is $2R_S = 4GM/c^2 = 8.4$ mas. The silhouette diameter without rotation ($a = 0$) is $(108)^{0.5} GM/c^2 = 22$ mas. The silhouette diameter for limiting rotation ($a = 1$) is $9GM/c^2 = 19$ mas, the image shift is $(5)^{0.5} GM/c^2 = 4.9$ mas. The halfwidth of the Radioastron beam is 7 mas.

one-sided relativistic jet. One possible explanation of such a structure is that it is not a supermassive black hole but a wormhole entrance [15–18].

For the polarization measurements of both objects presented in Fig. 7, their magnetic field structure near the central source must be known. Is it dipole or monopole? Or maybe even more complicated? If the magnetic field is due to an accretion disk around the central black hole, a dipole structure of the field is expected. Measurements of the Faraday rotation reported in [14] suggest that the opposite edges with respect to the central source rotate in the opposite sense and hence have the opposite direction of the magnetic field. This may imply a monopole structure of the magnetic field, as expected near the entrance to a wormhole or near a black hole with a magnetic charge (a former wormhole).

Cosmic ray sources are also an important research field. Figure 8 demonstrates the results of observations carried out by the Pierre Auger array [19]. Most ultrahigh-energy cosmic ray particles are discovered to come to Earth from the nearby radio galaxy Centaurus A (NGC5128) located at the distance 3.5 Mpc, which harbors a black hole with the mass of 5.5×10^7 solar masses, i.e., ten times smaller than M87. It is shown that powerful extragalactic synchrotron sources are simultaneously sources of ultrahigh-energy cosmic rays; in these sources, ultrarelativistic protons can therefore generate synchrotron radio emission that can be observed [20]. The characteristic frequency of the synchrotron radiation of a relativistic particle is

$$\nu_c = \frac{3}{4\pi} \frac{eH_\perp \gamma^2}{mc}, \qquad (1)$$

where $H_\perp$ is the projection of the magnetic field strength normal to the line of sight and γ is the Lorentz factor. If the synchrotron radiation is due to a dipole magnetic field line

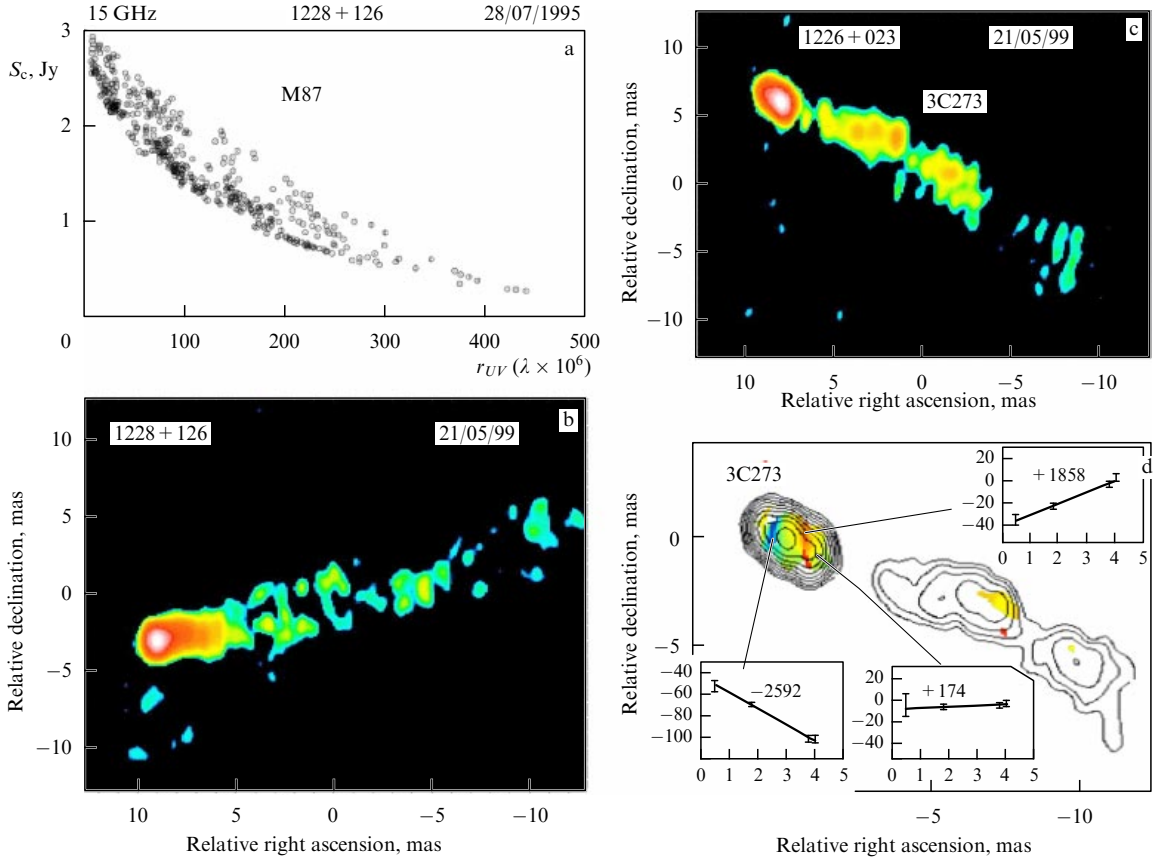

Figure 7. Physics near the black hole horizon or the entrance to a wormhole. M87 and 3C273 are the 'rosetta stones' for the Radioastron studies. (a) The radio flux S_c from M87 detected by VLBA at 2 cm as a function of the baseline projection r_{UV} on the UV-plane in the sky. (b) Radio image of M87. (c) Radio image of 3C273. (d) Rotation of the polarization plane for different parts of the 3C273 image; insets show the linear polarization position angle (in degrees) as a function of frequency (in MHz); figures in the insets show the rotation measure in rad m^{-2}.

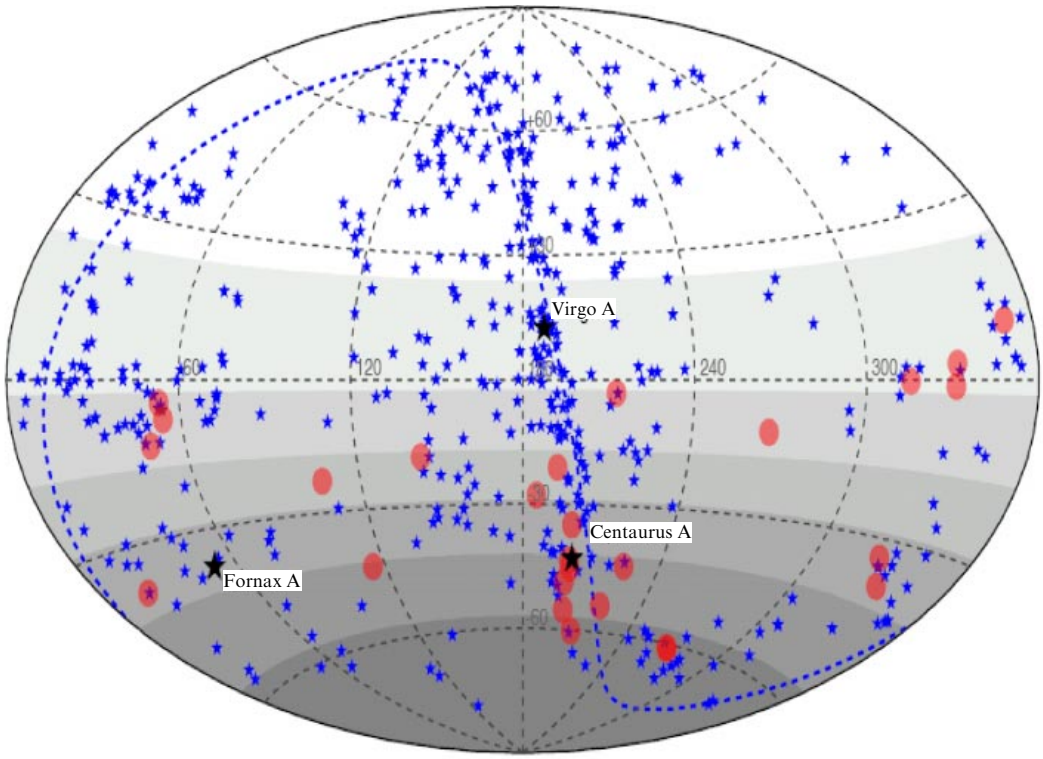

Figure 8. The location of 27 sources of ultrahigh-energy cosmic rays in the sky (in the equatorial coordinates) obtained by the AUGER array (dark circles) and 472 nearby ($z < 0.018$) active galaxies (asterisks) [19].

curvature, then the characteristic frequency is

$$\nu_c = \frac{9}{16\pi}\,\frac{cr\gamma^3}{R^2}\,, \tag{2}$$

where r and R are the respective distances from the emitting particle to the dipole axis and its center.

The ratio of the limiting brightness temperatures for relativistic protons and electrons (if the intensity is limited by Compton scattering of the same emission) is

$$\frac{T_p}{T_e} = \left(\frac{m_p}{m_e}\right)^{6/5} = (1830)^{6/5} = 8821\,. \tag{3}$$

If the limiting temperature of the synchrotron radiation of relativistic electrons is $T_e = 10^{12}$ K, the expected limiting synchrotron temperature of relativistic protons is $T_p = 8 \times 10^{15}$ K. For a given radiation flux $F_\nu \propto (T/\lambda^2)\Omega \propto T/B^2$, where T is the brightness temperature and Ω is the solid angle of the source. If B_e and B_p are projections of the interferometer baseline in the sky for emitting electrons and protons, needed to resolve the source with a given flux at the limiting brightness temperatures, then their ratio is

$$\frac{B_p}{B_e} = \left(\frac{m_p}{m_e}\right)^{3/5} = 90\,. \tag{4}$$

This means that resolving proton synchrotron sources may require interferometers with much longer baselines than for electrons.

The results of calculations in [20] show that if cosmic ray acceleration sites are associated with compact regions of the observed extragalactic radio sources, then the synchrotron radiation of relativistic protons can be detected from

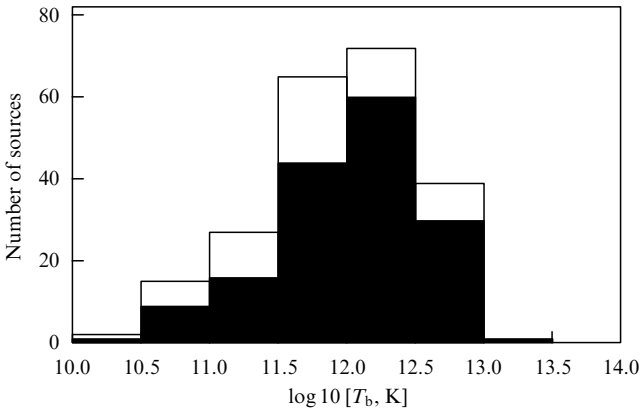

Figure 9. The histogram of brightness temperatures obtained from the survey of 242 extragalactic radio sources [21].

observations of very high brightness temperatures exceeding the electron synchrotron limit. In these observations, the brightness temperature excess due to the source motion toward the observer (the Doppler boost) resulting from its proper motion or expansion must be taken into account.

Figure 9 shows the histogram of brightness temperatures of sources observed by the VSOP space interferometer (VLBI Space Observing Program) at the 6 GHz band [13, 21]. A significant fraction (more than half) of the sources demonstrate a brightness temperature above 10^{12} K, i.e., the emission can be generated by relativistic protons. However, as we have noted, there also exist other models related to the motion of the emitting region and hence to the radiation directivity and an increase in the brightness temperature. Only the use of high angular resolution allows clarifying

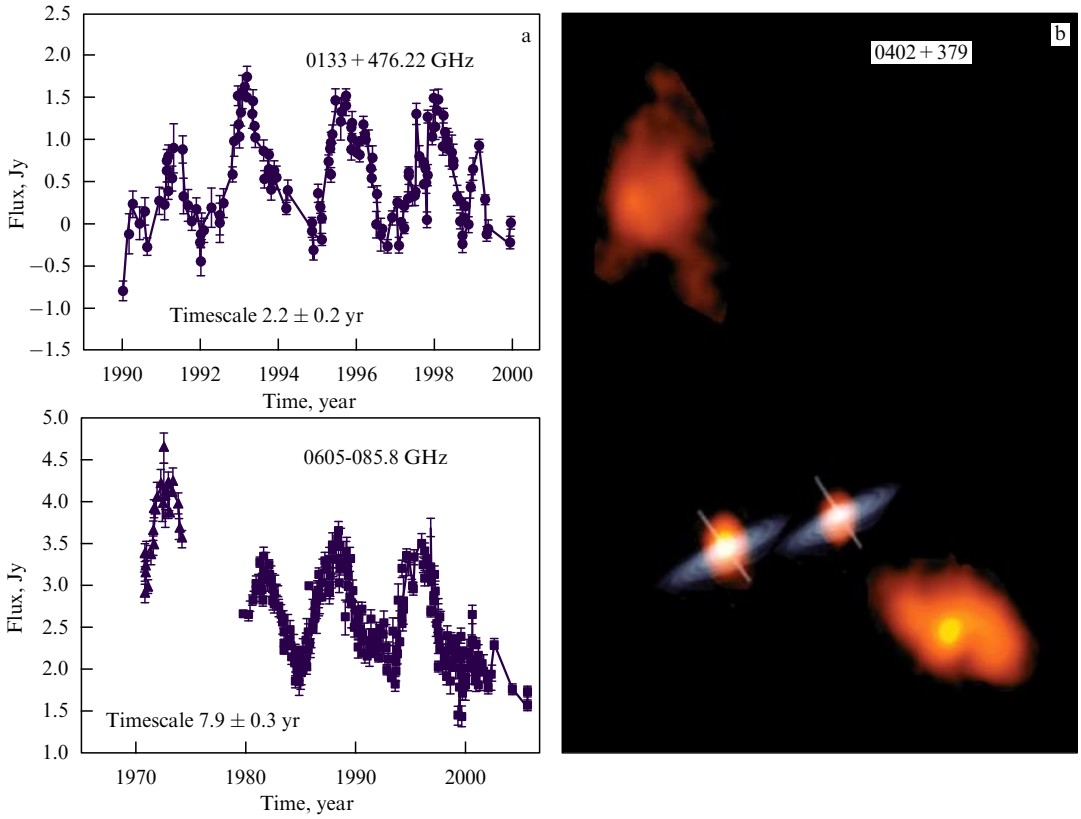

Figure 10. (a) Periodic flux variations from objects 0133+476 and 0605-085. (b) Radio galaxy 0402+379, $z = 0.055$, the distance between components is 7 mas; observed by VLBA at the frequency 15 GHz [24, 25].

whether a steady synchrotron source with high brightness temperature, e.g., 10^{15} K, is indeed observed. The discovery of such a source would confirm that a real cosmic ray generator exists there and its properties can be studied.

Many extragalactic sources are observed to show strong radio flux variability. These observations also allow determining the lower limit of the brightness temperature. For example, the intraday variability observed in the source 0716+714 implies the brightness temperature greater than 10^{15} K and even 10^{19} K (!) [22, 23]. Such a brightness temperature in the model of Doppler boosting corresponds to the Lorentz factor 90, and this can be tested only by a space interferometer.

Figure 10 shows observations of the quasiperiodic flux variations [24, 25]. Periodic flux variability can be produced by binary supermassive black holes. Such possible sources are listed in Table 3. The structure, magnetic field, formation history, and evolution of these sources can be investigated by a space radio interferometer. The image of one such binary source is also presented in Fig. 10. The proper motion of the source components is not yet established, i.e., it is still unclear how this picture changes with time.

The possibility of using the ultrahigh angular resolution for fundamental cosmological problems can be related to measurements of the dependence of angular sizes of extragalactic radio sources or their proper motions on redshift. In Fig. 11, the crosses show the angular diameter of a radio source in redshift [26, 27]. Points to the left of this figure were obtained by a different method using brightness measurements of supernovae and recalculated for the corresponding angular size. The upper right point, which was also recalculated for the angular size of an extragalactic radio source, was

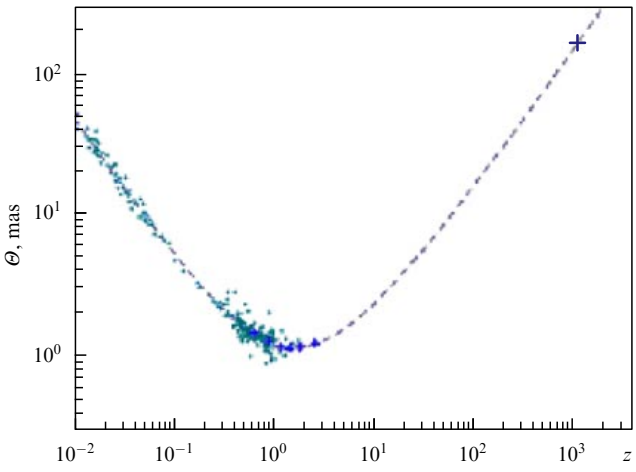

Figure 11. The angular diameter of radio sources Θ as a function of redshift for active galactic nuclei allows estimating the evolution of dark energy and dark matter and the sources themselves. Observations of 917 compact radio sources with fluxes above 0.5 Jy at the frequency 2.29 GHz were used. Each cross represents averaging over 77 sources. Points (source sizes) on the left side (see online figure at http://www.ufn.ru) were obtained from observations of supernovae. The upper right cross corresponds to the CMB acoustic horizon [26, 27].

obtained from measurements of the CMB space structure. But generally the entire plot is consistent with the standard cosmological model and allows refining its parameters. Extragalactic sources occupy the most important part of this plot describing the location and shape of the minimum. The existing data can already be used to assess cosmological

Table 3. Some quasiperiodic and binary extragalactic radio sources.

IAU designation	Other names	z	Type	Observational period, years	S, Jy	Θ_{max}, mas	Θ_{min}, mas	T_b, 10^{13} K	N_0	N_c
0059+581		0.644	Q	4.5	2.72	0.13	0.11	> 0.12	1	0
0133+476	DA455	0.859	Q	2.2	4.21	0.22	< 0.03	> 2.06	6	3
0235+164		0.940	B	5.45	1.36	0.16	0.11	0.09	5	0
0605-085	OH-010	0.055	Q	7.9	0.83	0.69	< 0.11	> 0.02	5	5
0716+714		(0.3)	B		2.51	0.08	< 0.01	> 1.85	6	5
0851+202	OJ 287	0.306	B	11.64	3.32	0.12	< 0.05	> 0.39	10	7
1219+044	ON231	0.965	Q	6.80	0.92	0.19	0.12	0.009	7	4
1226+023	3C273	0.158	Q		7.36	0.13	< 0.06	> 0.17	15	11
1253-055	3C279	0.538	Q	7.14	11.21	0.30	< 0.05	> 0.88	14	8
1641+399	3C345	0.594	Q	10.0	4.38	0.20	0.04	0.54	12	6
1803+784		0.680	B		1.62	0.15	0.08	0.125	8	0
2200+420	BL Lac	0.069	B	8	2.78	0.37	< 0.03	> 0.15	14	10
2223-052	3C446	1.404	Q	4.2	2.72	0.22	< 0.04	> 0.65	9	7
2230+114	CTA 102	1.037	Q		3.11	0.12	< 0.03	> 1.27	9	5
2251+158	3C454.3	0.859	Q	12.8	3.77	0.26	0.11	0.105	11	4

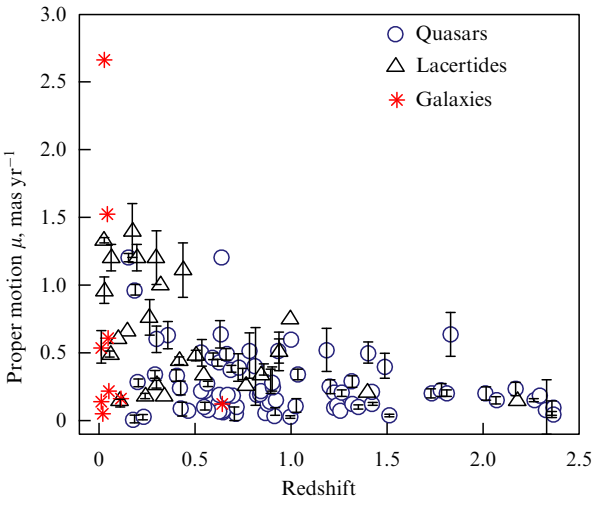

Figure 12. Proper motion of 'superluminal' jets from active galactic nuclei as a function of redshift [29].

parameters in an independent way. Observations with high angular resolution may allow refining this dependence and finding more precise values of the cosmological parameters, including dark energy and dark matter content and their evolution.

As we noted, observations show that many extragalactic radio sources change their form and size and demonstrate high angular velocities, which for a given distance to the source correspond to superluminal velocities. This effect is explained by the relativistic motion of the source. It is very important that the maximum proper motions of high-redshift sources can be measured (Fig. 12) [28]. This means that both nearby and remote objects can be studied and provides an independent method to determine cosmological parameters and to study the evolution of extragalactic objects.

To determine distances and cosmological parameters, it is also possible to use the well-known value and direction of the velocity of the Solar System relative to the CMB: $V = 369.0 \pm 0.9$ km s^{-1}, $l = 263.99° \pm 0.14°$, and $b = 48.26° \pm 0.03°$ [29], and measurements of the proper motions of extragalactic sources [30]. The Radioastron mission will allow such measurements for sources with redshifts about 0.05.

The topics of the Radioastron scientific program described above are related to studies of synchrotron sources within a broad frequency range. Narrow-band maser sources represent qualitatively different targets. A powerful narrow-band emission is observed in the lines of some molecules from star formation regions and protoplanetary systems. Figure 13 shows a model of such emission from a star formation region and the results of VLBA observations of the water vapor line at 22 GHz from the source W3(OH) [31]. The correlated flux (the ordinate) is plotted versus the interferometer baseline (the abscissa). It can be seen that the source is extremely compact and remains unresolved even for the largest baselines.

Also shown in Fig. 13 are maser sources emitting in the same line that are observed around the nucleus of galaxy NGC4258 [32]. Compact regions emitting in the water vapor line, which are observed around the central object (probably a black hole), are shown by dots. Red and blue dots (see the online version of Fig. 13 at http://www.ufn.ru) respectively mean the source motion toward or away from us. A class of such objects (megamasers) is observed. Individual details of megamasers remain unresolved and can be studied by a space interferometer. The expected limiting brightness temperatures amount to 10^{16} K [28].

In addition to resolving the structure of star formation complexes and measuring the size of individual regions, the measurements of parallaxes and proper motions of cosmic masers using the space interferometer are very important for modeling our Galaxy and other galaxies and for cosmological studies.

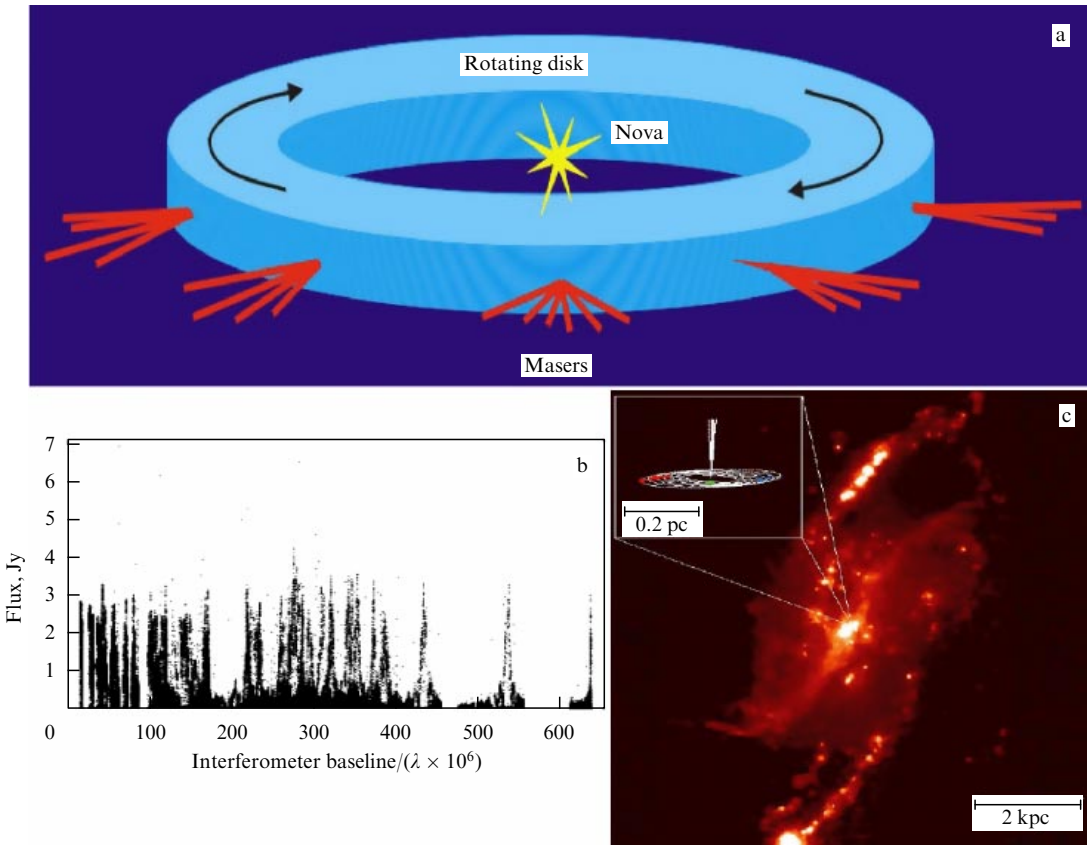

Figure 13. (a) The model of a star formation region with masers. (b) The observed VLA correlated flux from cosmic H_2O maser ($\approx$ 22 MHz) in the W3(OH) region as a function of the interferometer baseline (in millions of wavelengths, on abscissa) [31]. (c) H_2O megamaser and an image of galaxy NGC4258, distance 6.4 Mpc [32].

The coherent radiation mechanism provides even higher brightness temperatures. This mechanism is likely to be responsible for radio emission from pulsars (rotating neutron stars). But their sizes are so small that even a space interferometer would have insufficient angular resolution. Figure 14 shows a method that in fact has never been used in radio astronomy. It can be realized only in special observations with a space interferometer. The method anticipates observations of scintillations of the correlated signal produced by interstellar plasma inhomogeneities. Scintillations result from adding the signals that propagate through such a medium along different paths. This means that an interferometer with a huge baseline naturally emerges when a radio signal propagates through the interstellar plasma. In Fig. 14, we also show the results of 430 MHz Arecibo observations of interstellar scintillations from pulsar PSR1237+25 [33, 34] (the frequency as a function of time). The clear stripy picture corresponds to double-path signal propagation, i.e., to a two-antenna interferometer with a very long baseline; however, it is unclear so far what this picture looks like at different places in the near-Earth space. Such a sharp interference corresponding to the double-path ray propagation is rarely observed. Usually, a more complicated dynamic spectrum is seen corresponding to multipath signal propagation, but even in that case, it is possible to determine parameters of an effective interstellar interferometer [33, 34]. Using this method, an ultrahigh angular resolution exceeding that of the Earth-space interferometer by several hundred and even a thousand times may possibly be obtained by the Radioastron mission.

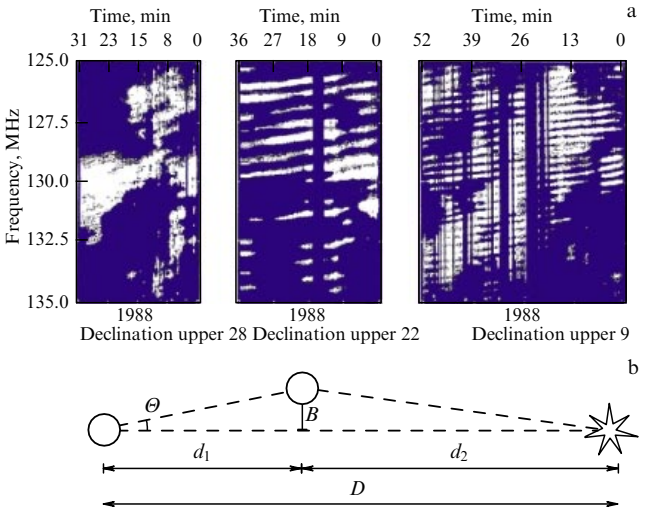

Figure 14. (a) Dynamic spectra of pulsar PSR 1237+25, period 1.4 s, distance 560 pc, Aresibo observations at the 430 MHz band [33, 34]. (b) the scheme of a double-beam 'interstellar' interferometer. B is the interferometer baseline, and d_1, d_2, and D are the respective distances between the observer and the interferometer, between the interferometer and the source, and the observer and the source.

Recently, a new class of pulsar magnetars (PSR J1550-5418, with the period 2.069 s, and XTE J1810-5408, with the period 5.54 s) was discovered. These pulsars show a spectrum that is anomalously flat and even increases with frequency in the cm and mm wavelength range [35, 36]. It is extremely

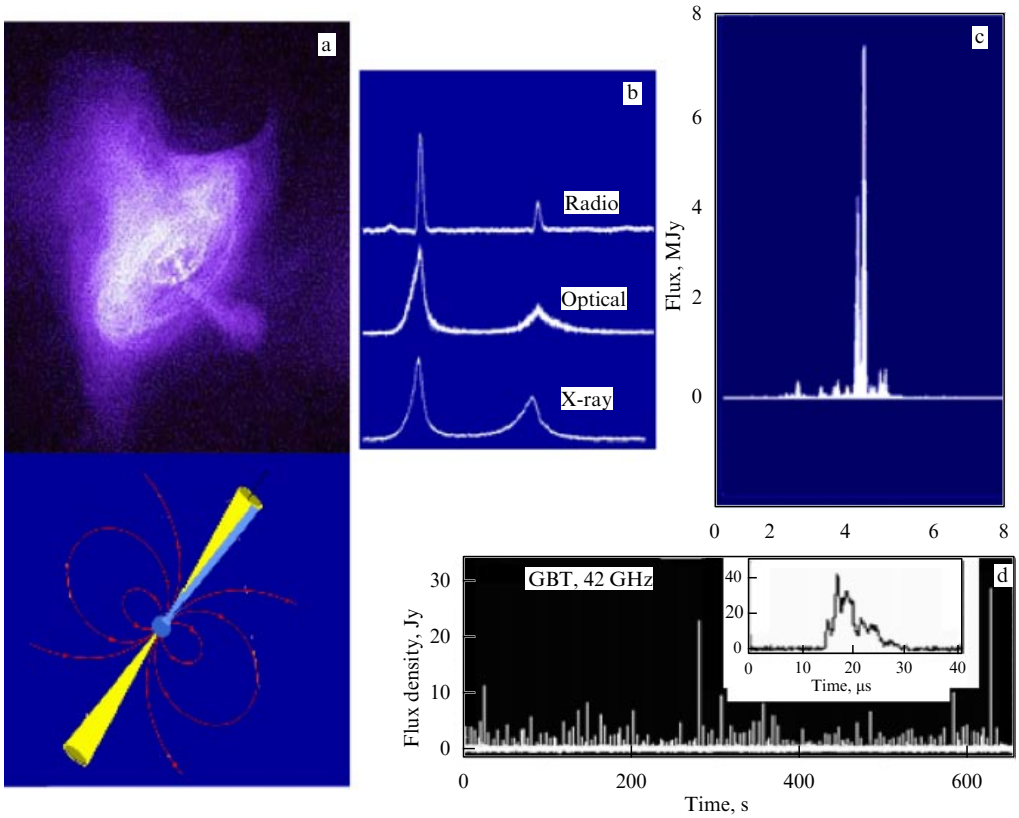

Figure 15. X-ray image of the Crab Nebula (the Chandra X-ray observatory) and the model of a rotating neutron star with a magnetic field. (b) Normal pulses (period 33 ms) in the radio, optical, and X-ray bands. (c) A supergiant radio pulse from the Crab Nebula: the flux near Earth is 7×10^6 Jy at 2.2 GHz with the brightness temperature $T > 10^{40}$ K and electromagnetic field $H > 10^{12}$ G; observations on RT-64 in Kalyazin [37, 38]. (d) The record of the source XTEJ1810-540 that sporadically shows up as a radio magnetar, period 5.54 s, magnetic field 2.6×10^{14} G; observations by GBT (Green Bank Telescope) at the frequency 42 GHz [35, 36].

interesting to know how coherent emission is generated at such high frequencies, i.e., how such small charge inhomogeneities can be produced. These objects simultaneously appear as transient X-ray sources. Their pulsating radio emission also appears sporadically. The results of observations of XTE J1810-540 are presented in Fig. 15d.

In several pulsars, individual giant pulses with amplitudes many orders of magnitude higher than the mean value have been discovered. In particular, in the Crab pulsar, such giant pulses are observed about once per hour (see Fig. 15). The absolute brightness temperature 10^{40} K was recorded in such giant pulses [37, 38]. In addition to the extremely interesting question as to where and how such pulses are generated in the neutron star magnetosphere, there is a very important application of observations of giant pulses: the time synchronization over the entire Earth using combined observations from many ground-based telescopes and the Radioastron space radio telescope.

The Radioastron mission will also study the Earth gravitational field based on the analysis of interferometric observations and high-precision measurements of the spacecraft orbit and evolution. These measurements include

• measurements of anomalous accelerations with an accuracy 10^{-10} m s^{-2} and the reconstruction of the gravitational potential of Earth at long distances;

• tests of general relativity effects (the transverse Doppler effect, time lapse, gravitational redshift measurements two orders of magnitude more precise, test of the $1/R^2$ law of the gravitational interaction, etc.).

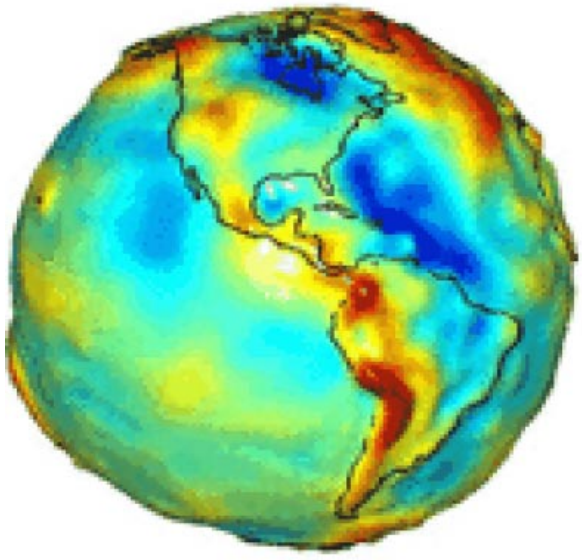

Figure 16. The map of gravity anomalies according to GRACE [39].

Figure 16 shows the map of gravity anomalies constructed from observations from the low-orbit GRACE (Gravity Recovery and Climate Experiment) satellite [39]. The Radioastron mission will be able to construct the Earth gravitational field at much larger distances.

Figure 17 illustrates the next mission after Radioastron: Millimetron [40, 41], which represents further development of

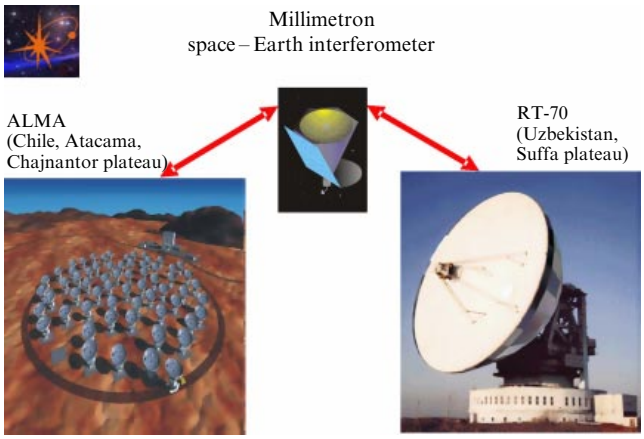

Figure 17. The Millimetron space observatory in the infrared and millimeter range [40, 41], the RT-70 radio telescope on the Suffa plain in Uzbekistan [42], and ALMA radio observatory in Chile [43].

this technique towards shorter wavelengths (millimeter and infrared bands covering the wavelength range from 20 mm to 20μm) with the help of a 12 m cryogenic reflector in orbit around the L_2 point (at the distance 1.5 mln km from Earth). The radio telescope RT-70 on the Suffa plateau (Uzbekistan) in the northern hemisphere and the ALMA (Atacama Large Millimeter/submillimeter Array) [43] on the Chajnantor plateau in Chile can be used in the southern hemisphere as the ground-based part of this space interferometer. ALMA is a large antenna array consisting of 68 reflectors 12 m in diameter operating at frequencies up to 1 THz, i.e., at the wavelength 300 μm. Generally, the Millimetron mission will be able to construct images of sources with the angular resolution given by several nano arcseconds (i.e., a few billion times the resolution of the human eye). In the autonomous regime, the interferometer will have a very high sensitivity, up to several nJy, due to deep cooling of the entire telescope to the temperature 4–5 K and even more deep cooling of the receivers.

It is planned that the Radioastron mission will be launched during the coming year. The duration of the mission will be more than five years. The Millimetron space observatory will be launched before 2020. The duration of the mission is assumed to be more than 10 years.

References

1. Salomonovich A E (Exec. Ed.) *Razvitie Radioastronomii v SSSR* (Development of Radio Astronomy in the USSR) (Moscow: Nauka, 1988)
2. Alekseev V A et al. *Sovetskie Radioteleskopy i Radioastronomiya Solntsa* (Soviet Radio Telescopes and solar Radio Astronomy) (Exec. Ed. A E Salomonovich, G Ya Smol'kov) (Moscow: Nauka, 1990)
3. Shklovsky I S *Iz Istorii Razvitiya Radioastronomii v SSSR* (From the History of Development of Radio Astronomy in the USSR) (Series New in Life, Science and Technics. Cosmonautics, Astronomy. Issue 11) (Moscow: Znanie, 1982)
4. Ginzburg V L *O Nauke, o Sebe i o Drugikh* (About Science, Myself, and Others) 3rd ed. (Moscow: Fizmatlit, 2003) p. 126 [Translated into English (Bristol: IOP Publ., 2005)]
5. RadioAstron, http://www.asc.rssi.ru/radioastron/index.html
6. Matveenko L I, Kardashev N S, Sholomitskii G B *Izv. Vyssh. Uchebn. Zaved. Radiofiz.* **8** 651 (1965) [*Radiophys. Quantum Electron.* **8** 461 (1965)]
7. Kardashev N S, Kreisman B B, Ponomarev Yu N, in *Radioastronomical Tools and Techniques* (Eds N S Kardashev, R D Dagkesamanskii) (Cambridge: Cambridge Sci. Publ., 2007) p. 3
8. Andreyanov V V et al., in *Radioastronomical Tools and Techniques* (Eds N S Kardashev, R D Dagkesamanskii) (Cambridge: Cambridge Sci. Publ., 2007) p. 17
9. Vol'vach A E, Vol'vach L N, Kardashev N S, Larionov M G *Astron. Zh.* **85** 483 (2008) [*Astron. Rep.* **52** 429 (2008)]
10. Mingaliev M G, Sotnikova Yu V, Bursov N N, Kardashev N S, Larionov M G *Astron. Zh.* **84** 387 (2007) [*Astron. Rep.* **51** 343 (2007)]
11. Kovalev Y Y et al. *Astron. J.* **130** 2473 (2005)
12. Kellermann K I et al. *Astrophys. J.* **609** 539 (2004)
13. Broderick A E, Loeb A, arXiv:0812.0366
14. Zavala R T, Taylor G B *Astrophys. J.* **550** L147 (2001)
15. Kardashev N S, Novikov I D, Shatskii A A *Astron. Zh.* **83** 675 (2006) [*Astron. Rep.* **50** 601 (2006)]
16. Shatskii A A, Novikov I D, Kardashev N S *Usp. Fiz. Nauk* **178** 481 (2008) [*Phys. Usp.* **51** 457 (2008)]
17. Novikov I D, Kardashev N S, Shatskii A A *Usp. Fiz. Nauk* **177** 1017 (2007) [*Phys. Usp.* **50** 965 (2007)]
18. Kardashev N S *Usp. Fiz. Nauk* **177** 553 (2007) [*Phys. Usp.* **50** 529 (2007)]
19. Bluemer J for the Pierre Auger Collab., arXiv:0807.4871
20. Kardashev N S *Astron. Zh.* **77** 813 (2000) [*Astron. Rep.* **44** 719 (2000)]
21. Dodson R, Fomalont E, Wiik K, arXiv:0901.1493
22. Bach U et al., arXiv:0802.3823
23. Fuhrmann L et al., arXiv:0809.2227
24. Krichbaum T, http://www.mpifr-bonn.mpg.de/div/vlbi/vsop2bonn/pdf/krichbaum.pdf
25. Rodriguez C et al. *Astrophys. J.* **646** 49 (2006)
26. Jackson J C, Jannetta A L *JCAP* **0611** 002 (2006); astro-ph/0605065
27. Jackson J C *Mon. Not. R. Astron. Soc.* **390** L1 (2008); arXiv:0810.3930
28. Zhang Y-W, Fan J-H *Chin. J. Astron. Astrophys.* **8** 385 (2008)
29. Hinshaw G et al. *Astrophys. J. Suppl.* **180** 225 (2009)
30. Kardashev N S *Astron. Zh.* **63** 845 (1986) [*Sov. Astron. Rep.* **30** 501 (1986)]
31. Slysh V I *ASP Conf. Proc.* **300** 239 (2003)
32. Miyoshi M et al. *Nature* **373** 127 (1995)
33. Wolszczan A, Cordes J M *Astrophys. J.* **320** L35 (1987)
34. Shishov V I *Astron. Zh.* **78** 229 (2001) [*Astron. Rep.* **45** 195 (2001)]
35. Camilo F et al. *Nature* **442** 892 (2006); astro-ph/0605429
36. Camilo F et al. *Astrophys. J.* **669** 561 (2007)
37. Popov M V et al., arXiv:0903.2652
38. Soglasnov V, astro-ph/0701190
39. Gravity Recovery and Climate Experiment, http://nasascience.nasa.gov/missions/grace/
40. Millimetron Project, http://www.asc.rssi.ru/millimetron/eng/millim_eng.htm
41. Wild W, Kardashev N (On behalf of the Millimetron consortium) *Exp. Astron.* **23** 221 (2009); http://www.springerlink.com/content/621161q85n614328/fulltext.pdf
42. The RT-70 radio telescope of the International Radioastronomical Observatory on 'Suffa' plain, http://www.asc.rssi.ru/suffa
43. Wootten A, Thompson A R *Proc. IEEE* **97** 1463 (2009); arXiv: 0904.3739